Available online at www.sciencedirect.com
SCIENCE DIRECT
Journal of the European Ceramic Society 26 (2006) 1507–1515
www.elsevier.com/locate/jeurceramsoc

Physical properties of 8 mol% Ceria doped yttria stabilised zirconia powder and ceramic and their behaviour during annealing and sintering

A.A. Bukaemskiy, D. Barrier *, G. Modolo

Institut für Sicherheitsforschung und Reaktortechnik, Forschungszentrum Jülich GmbH, 52425 Jülich, Germany

Received 9 November 2004; received in revised form 28 January 2005; accepted 4 February 2005
Available online 16 March 2005

Abstract

The thermal behaviour of 8 mol% Ceria doped 16 mol% yttria stabilised zirconia (Ce-YSZ) powder, synthesised by the wet co-precipitation method, has been investigated in details. The lattice parameter, mean crystallite size and lattice distortions have been determined as a function of calcination temperature. After grinding by attrition followed by fractionating in acetone, the powders were compacted and sintered at 1600 °C in air for 5 h. The sintering behaviour of pellets was studied by dilatometry, revealing different sintering behaviour depending on the calcination temperature of the powders and the type of agglomerates. The influence of these latter parameters on the microstructure of pellets has been investigated. The pellets produced from powders calcined at low-temperature, from 110 to 600 °C, present the highest densities and the best morphological structure.

Keywords: Calcination; X-Ray methods; Microstructure; ZrO_2–Y_2O_3–CeO_2; Nuclear application

1. Introduction

In recent years, yttria stabilised zirconia has been considered as an attractive matrix for nuclear application, such as inert fuel for the destruction of excess of Plutonium or a good host material for nuclear waste storage.[1–3] In fact, this material has a high leaching resistance, a high radiation stability, a small neutron capture cross section and a high melting point.[4,5] Furthermore, this system has the ability to form solid solutions, in a wide range of solubility, with compounds such as UO_2, ThO_2 and PuO_2.[4] In ceramic research these radioactive oxides are substituted by surrogates such as CeO_2 or other lanthanides.

The ternary system ZrO_2–Y_2O_3–CeO_2 has been studied in detail.[6,7] However, a lot of questions about crystallisation peculiarities and evolution of crystal structure with temperature are not clearly understood.

Moreover, the influence of annealing and further production steps (milling, fractionating, pressing) on the material sintering behaviour and the properties of the final ceramic have a great scientific and practical interest, particularly for nuclear applications, which require simple and dust-free technological methods for ceramic production.[1] In this case many traditional powder technologies are either not efficient or need special adaptation. Therefore, “mild” methods of powder preparation, such as grinding by attrition in solvent, followed by calcination at low temperature, are mainly considered for processing of radioactive materials.

In this context wet chemical processes of multication oxides, such as co-precipitation method, are attractive. In fact, in addition to their simplicity, the latter methods provides considerable advantages of good mixing of the starting material and excellent chemical homogeneity of the final product. However, one main disadvantage of co-precipitation method is that ultrafine particles undergo severe agglomeration during drying. These powders are very sensitive to the calcination temperature, which increase their crystallinity and

* Corresponding author. Tel.: +49 2461 612752; fax: +49 2461 612450.
E-mail address: d.barrier@fz-juelich.de (D. Barrier).

0955-2219/$ – see front matter © 2005 Elsevier Ltd. All rights reserved.
doi:10.1016/j.jeurceramsoc.2005.02.002

lead to harder agglomerates that can strongly influence their sinterability.[8,9]

In the present work, the possibility of producing pellets with properties required for nuclear application using a simple and dust-free process, adapted for handling radioactive material, has been investigated. The morphology of 8 mol% Ceria doped 16 mol% yttria stabilised zirconia (Ce-YSZ) powder, its thermal behaviour and the peculiarities of material crystallisation have been investigated by scanning electron microscopy (SEM), thermogravimetry coupled with differential scanning calorimetry (TG-DSC) and X-ray diffractometry (XRD). The influence of the calcination temperature on the sinterability of pellets and the role of agglomerate type during sintering was studied in detail using dilatometry.

2. Experimental procedure

2.1. Synthesis of Ce-YSZ powder and pellets

The Ce-YSZ powder was synthesised by the co-precipitation method. The addition of 16 mol.% of yttrium oxide to the system allows stabilisation of zirconia matrix in cubic phase.[6] $ZrOCl_2{\cdot}8H_2O$, $Y(NO_3)_3{\cdot}6H_2O$ and $Ce(NO_3)_3{\cdot}6H_2O$ supplied by Alfa Aesar with a purity of 99.9% were used as initial materials. The required quantity of the chemicals was dissolved in deionised water at room temperature. On stirring, ammonia gas was used for the co-precipitation. The same procedure was used for obtaining $(Zr_{0.84}Y_{0.16})O_{1.92}$ (16-YSZ) reference powder.

The precipitates were separated and carefully washed by deionised water until ammonium, nitrate and chloride were completely eliminated and finally dried at 110 °C for 24 h. Afterwards the powders were calcined in air at calcination temperatures (T_C of 350, 500, 600, 800, 950, 1400 and 1600 °C).

Before sintering, the powders were ground by attrition using a Mortar Grinder KM 100 from Retsch. To prevent dust formation, grinding was performed in acetone. Then the powders were eventually fractionated in acetone and agglomerates with an equivalent diameter less than 4 μm were collected.[10]

Finally the powders (approximately 1 g) were compacted by cold uniaxial pressing into cylindrical pellets of 10 mm diameter. The range of pressures used varied from 300 to 1000 MPa depending on the powders calcination temperature. For each powder, the optimal compacting pressure was determined as reported in previous work.[11] The pellets were then sintered in a resistance heated furnace at 1600 °C in air atmosphere for 5 h, using a heating rate of 3 K/min.

2.2. Characterisation

Thermal behaviour of the powders during heating from room temperature to 1400 °C was investigated by TG-DSC in air or nitrogen with a heating rate of 10 K/min using a Netzsch STA 449C Jupiter apparatus.

The crystal structure of the powders and sintered pellets was investigated XRD using a Stoe Transmissions-Diffractometer-System STADI (Co Kα, $\lambda = 0.178897$ nm). To evaluate the mean crystallite size L and the lattice distortions $\langle\varepsilon^2\rangle^{0.5}$ from XRD measurements, the Hall–Williamson method was used[12]:

$$\beta\cos(\theta) = \frac{\lambda}{L} + 4\langle\varepsilon^2\rangle^{0.5}\sin(\theta) \quad (1)$$

where θ is the Bragg angle of diffraction, λ the wavelength of incident X-rays (0.178897 nm) and β is the peak half-width corrected to instrumental widening.

The values $\beta\cos(\theta)$ calculated for each peak were plotted as a function of $\sin(\theta)$. The linear regression of the obtained data allows the determination of the mean crystallite size L and lattice distortions $\langle\varepsilon^2\rangle^{0.5}$.

The mean crystallite size of amorphous powders were determined by using the Scherrer formula applied on the diffraction plan $\langle 1\,1\,1\rangle$,[13] where K is a shape factor ($K = 0.9$):

$$L = \frac{K\lambda}{\beta\cos(\theta)} \quad (2)$$

The morphological structures of powders and pellets were investigated by (SEM). The particles size distribution was studied by laser granulometry (Quantachrom, Cilas 920)

The pellets densities were determined by the geometrical method for the green bodies and by the hydrostatic weighing method in water for the sintered bodies. The theoretical densities of the materials (ρ_T) were calculated from the results of the XRD measurements.

The sintering behaviour of the pellets was studied by dilatometry (Netzsch DIL 402C). After compaction, the pellets were heated from room temperature to 1600 °C, with a heating rate of 3 K/min.

3. Results and discussion

3.1. Physical properties of the powder

After drying the 16-YSZ and Ce-YSZ powders are white and yellow, respectively. After grinding by attrition in acetone and drying at 110 °C, the morphology of Ce-YSZ powder was analysed by SEM, which revealed agglomerates with irregular shape and variable packing density of their primary particles (Fig. 1). According to literature,[14] these agglomerates can be classified as “soft” or “hard”, the “hard” agglomerates consisting of close-packed particles with high densities.

After drying at 110 °C in air for 12 h the Ce-YSZ and the 16-YSZ reference powders were investigated by thermal analysis (TG-DSC) in air (Fig. 2). During heating from 25 to 660 °C a significant mass loss (12.2%) was revealed. From 25 to 370 °C, it is accompanied by the heat consumption which corresponds to the elimination of adsorbed gases, adsorbed and crystal water. In the temperature region from 370

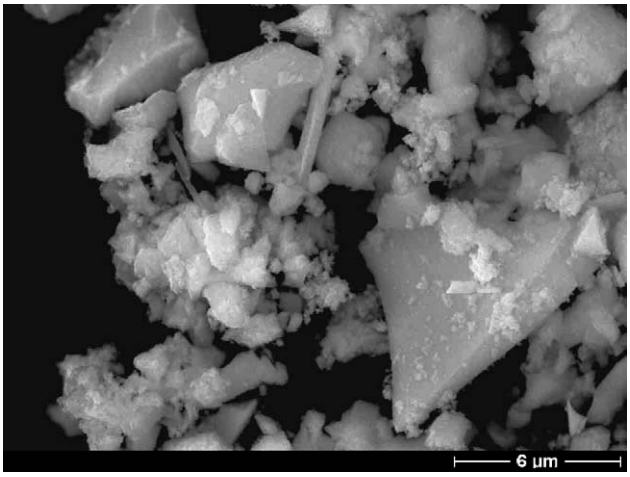

Fig. 1. SEM image of Ce-YSZ powder after drying at 110 °C and grinding by attrition.

to 660 °C, the mass loss is accompanied by complex exo-effects (Fig. 2).

According to literature, the thermal effects observed on the DSC curve at 370–660 °C can correspond either to a crystallisation of material[15,16] or to a valence change of cerium (Ce(III) → Ce(IV)).[17] In order to determine whether the latter mechanism is prevailing, thermal analysis of the powder was performed in this temperature range in inert atmosphere (nitrogen). The DSC curve reveals between 370 and 660 °C two similar exo-effects as observed in air. So it can be concluded that both exothermic peaks do not correspond to a valence change but are correlated to a crystallisation of material.

The crystallisation of the Ce-YSZ system include two exothermic peaks, respectively characterised by their specific heats Q_1 and Q_2. As described in Fig. 2, the first effect is detected between 370 °C (T_1) and 502 °C (T_3) with a maximum at 445 °C (T_2). The second effect is detected between 502 °C (T_3) and 660 °C (T_5) with a maximum at 568 °C (T_4). The specific heat of the first peak (Q_1 = 33.9 J/g) is higher than the specific heat of the second peak (Q_2 = 20.7 J/g).

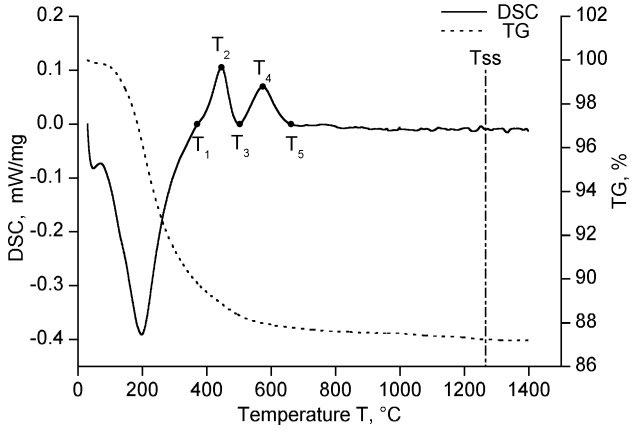

Fig. 2. TG and DSC curves of Ce-YSZ powder in air atmosphere.

The thermal behaviour of the reference sample 16-YSZ was also investigated and is similar to that of the Ce-YSZ powder. The only difference appears in the temperature range of crystallisation. The DSC curve of the reference sample presents only one exo-effect between 420 °C (T_1^R) and 525 °C (T_3^R). The maximum of this effect is detected at 458 °C (T_2^R) and the total specific heat of the effect has a value of 111.3 J/g.

During subsequent heating from 660 up to 1400 °C, for both materials, no thermal effects were observed on the DSC curves. On contrary, in this temperature range, the mass of the sample still slowly decreases until 1265 °C and then remains constant until 1400 °C. The mass loss in the temperature range from 370 up to 1265 °C can be associated with elimination of OH-groups from material.[18]

According to the TG and DSC results, the Ce-YSZ powder was calcined at 370, 450, 500, 550, 600, 800, 950, 1400 and 1600 °C before XRD analysis. The yellow colour characteristics of the cerium addition remains for all calcination temperature. For powders after drying and calcination at temperatures below 370 °C (T_1), no diffraction peaks are observed on the XRD spectra in Fig. 3; the powders are amorphous. At temperatures higher than T_1, the diffraction peak of XRD

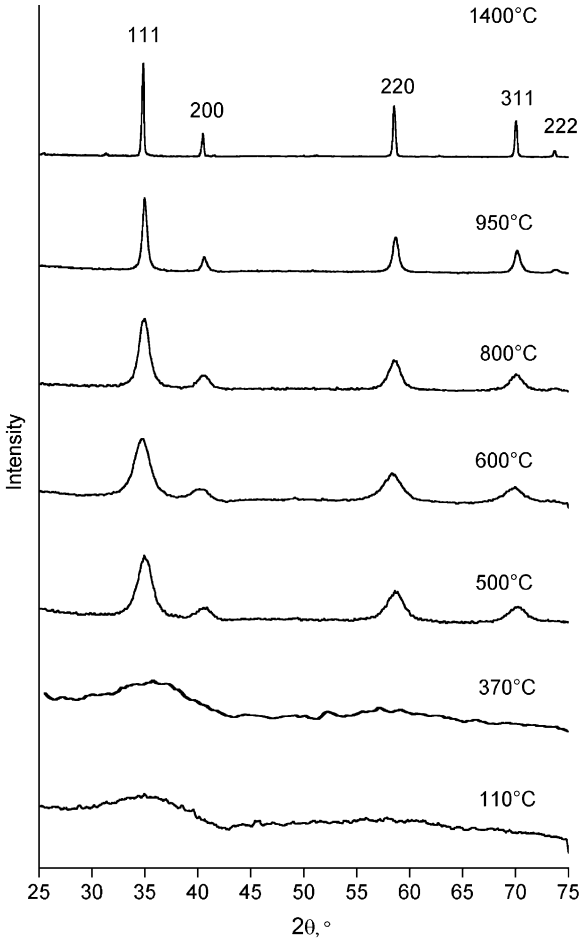

Fig. 3. Powder X-ray diffractograms for Ce-YSZ powders after drying at 110 °C and calcination at 370, 500, 600, 800, 950 and 1400 °C.

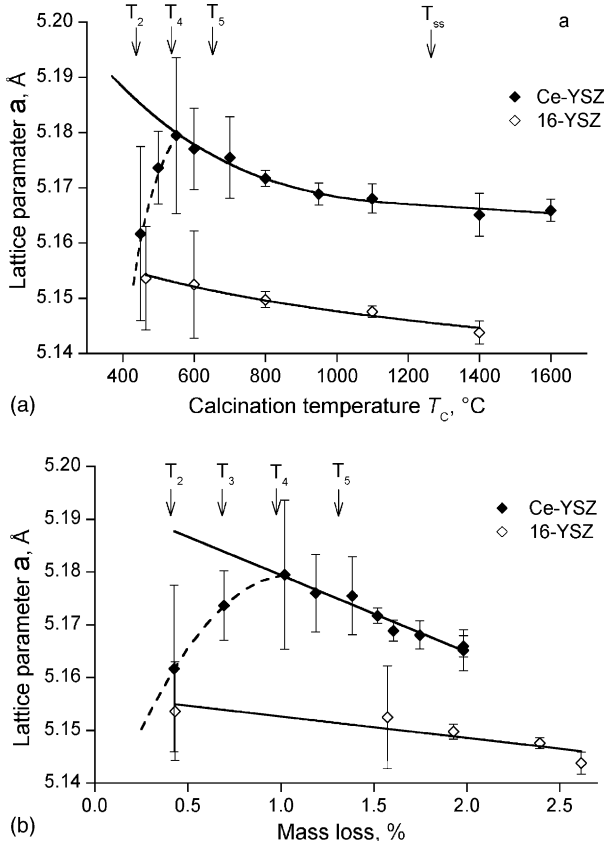

Fig. 4. Dependence of the lattice parameter with the calcination temperature (a) and the mass loss (b).

spectra reveal that the material crystallises in a face-centred cubic fluorite-type structure. For powders calcined from 450 to 950 °C, diffraction lines are wider and shifted in the smaller angels region compared to those for the powders calcined at 1400 and 1600 °C. At temperatures higher than 1265 °C, the material transforms into a stable solid solution. In the following this temperature (1265 °C) will be termed as T_{ss} (temperature of stable solid solution formation).

The dependence of the lattice parameter a of Ce-YSZ and 16-YSZ on the calcination temperature (Fig. 4a) and on the mass loss (Fig. 4b) was investigated in details.

For both materials, the lattice parameter decreases with increasing calcination temperature (Fig. 4a) and the mass loss (Fig. 4b). At the temperature higher than $T_3 = 502$ °C and $T_1^R = 420$ °C for Ce-YSZ and 16-YSZ, respectively, the lattice parameter has a linear correlation with the sample mass loss $(M_{T_1} - M_T)/M_{T_1}$ (Fig. 4b). In this formula, M_T is the sample mass at the temperature T and M_{T_1} the sample mass at the beginning of the phase transition ($T_1 = 370$ °C for Ce-YSZ system or $T_1^R = 420$ °C for the reference sample). This linear correlation confirms that the lattice parameter is determined by the presence of OH-groups in the material.[18]

In contrast, the Ce-YSZ samples calcined at the lower temperatures $T_2 = 450$ °C and $T_3 = 502$ °C do not follow the above tendencies with the calcination temperature and the mass loss (Fig. 4a and b). Their lattice parameters ($a_{T_2} = 5.162$ Å and $a_{T_3} = 5.174$ Å) are significantly lower than the values extrapolated from the higher temperatures ($a_{T_2}^{ext} = 5.185$ Å and $a_{T_3}^{ext} = 5.182$ Å). Moreover, after calcination at 450 °C, the values of the lattice parameter of Ce-YSZ and 16-YSZ ($a = 5.162 \pm 0.016$ Å and $a^R = 5.154 \pm 0.009$ Å, respectively) are very similar (Fig. 4a and b).

It is known that ceria forms a homogeneous solid solution with yttrium fully stabilised Zirconia[6] and that the lattice parameter of the $[(Zr_{0.84}Y_{0.16})_{1-y}Ce_y]O_{2-x}$ system increases linearly with the addition of ceria following the Vegard's Law[3,19] also after calcination at lower temperatures.[20] So, it can be concluded that the low value of the lattice parameter at temperature lower than T_3 is connected with the deficiency of ceria in the crystallised material.

Hence, taking into account the TG-DSC and XRD results, the following sequence of material crystallisation can be assumed: predominant crystallisation of zirconia–yttria matrix with the ceria deficiency in the temperature range from T_1 to T_3 (first exo-effect) and incorporation of the rest of ceria in the crystal lattice in the temperature range from T_3 to T_5 (second exo-effect).

According to the work of Kinoshita et al.,[21] Ce-YSZ system crystallise in fluorite structure, independently of the oxidation degree of cerium, if the ceria content is less than 15 mol %. However, Ce(III) was detected in the Ce-YSZ system only if it is sintered in reducing atmospheres. In the present case of the 8 mol% Ceria doped 16-YSZ powder, the lattice parameter of this material is located on the straight line defined between the lattice parameter of YSZ and pure CeO_2 (a_{CeO_2}, Å $= 5.4113 \pm 0.0012$).[22] This fact confirm that Ce(IV) is in majority present in the 8 mol% Ceria doped 16-YSZ synthesised material.[21]

The mean crystallite size and the lattice distortions of Ce-YSZ were also determined from XRD results. The mean crystallite size L increases from 2 to 135 nm while the lattice distortions $\langle\varepsilon^2\rangle^{1/2}$ decrease from 0.5 to 0.04% with increasing calcination temperature (Fig. 5). After drying at 110 °C, the crystallite size is very small ($L \sim 2$ nm) and represents the pri-

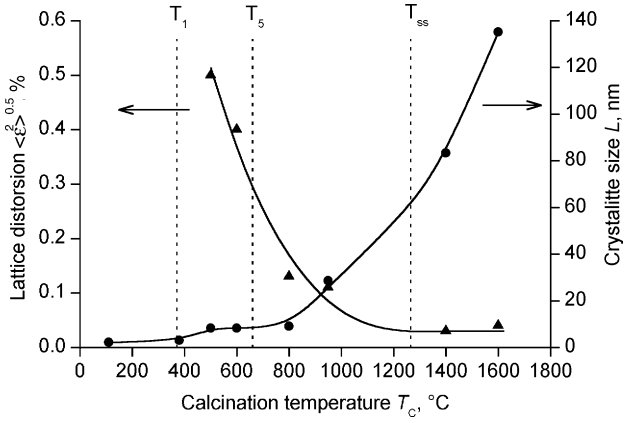

Fig. 5. Evolution of the mean crystallite size (▲) and the lattice distortion (●) as a function of the calcination temperature.

mary particle size produced by the co-precipitation method.[18] During the drying step, the particles form large agglomerates due to their high adhesion activity after the evaporation of water (Fig. 1).

During the phase transition from amorphous to crystallite which occur at T_1–T_5, the mean crystallite size L increases up to ~8 nm. In this temperature region, the material is characterised by a high level of lattice distortion $\langle\varepsilon^2\rangle^{0.5} \sim 0.4$–$0.5\%$, which is due to the presence of OH-groups in the matrix and the lattice rearrangement from amorphous to crystallite state.

Heating the material above 800 °C is responsible for the material recrystallisation, which results in a steep increase of the crystallite size up to 135 nm and decrease of lattice distortion. Heating the material at temperature higher than T_{ss} results in lattice stress relaxation and in crystallisation of the material in to a stable phase. This reduces the lattice distortions to virtually zero.

3.2. The physical properties of the pellets

To study the influence of calcination temperature on the compressibility of powders, they were first ground by attrition in acetone and then pressed into pellets at different pressures.

At fixed pressure (for example, in Fig. 6, $P = 1020$ MPa), the density of the green bodies linearly increases from 0.45 to 0.69 of the theoretical density (TD) with increasing the powders calcination temperature from 110 to 1400 °C. This effect can be associated to the evolution of particle morphology resulting from the elimination of OH-groups and the recrystallisation of material during calcination.

Each powder was pressed at an optimal compacting pressure, determined experimentally[11] and the pellets were then sintered at 1600 °C for 5 h. For a better dehydration of the pellets, a slow heating rate of 3 K/min was used.

After sintering, all pellets have a pale yellow colour. The dependence of the sintered densities on the calcination temperature (Fig. 7) clearly shows that the powder has a better sinterability when it was calcined at low calcination temperature (from 110 to 600 °C). In this case the density of pellets reaches a value of 0.92 TD. On contrary, if the powder is calcined at 800 °C and higher, the density of the sintered pellets decreases to 0.84 TD.

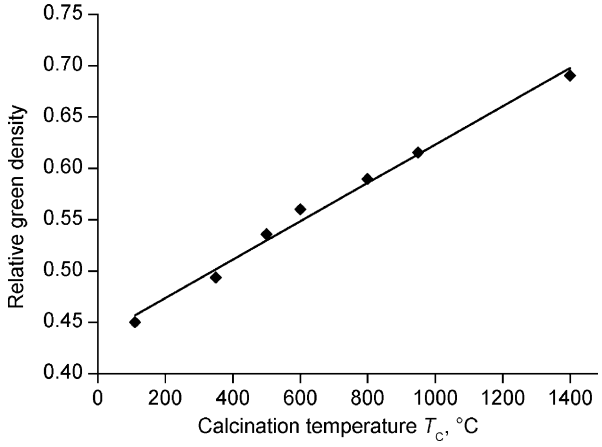

Fig. 6. Relative green density of Ce-YSZ pellets in dependence on the calcination temperature. All pellets were compacted at 1020 MPa.

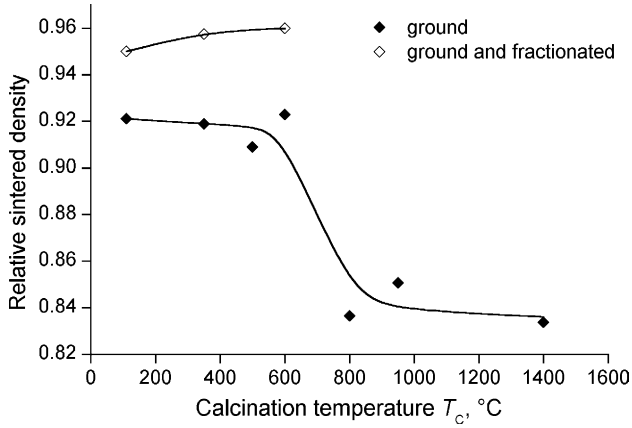

Fig. 7. Dependence of relative sintered densities of Ce-YSZ pellets made from ground (♦) and fractionated (◊) powder, on calcination temperature.

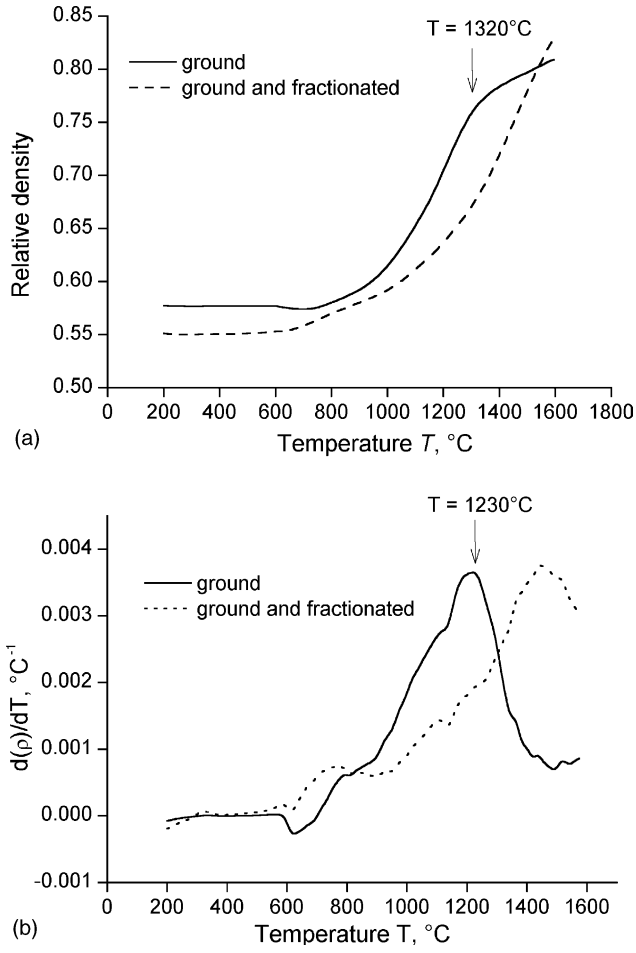

Fig. 8. Evolution with the annealing temperature of the relative density R_d (a) and its derivative $d(R_d)/dT$ (b) of Ce-YSZ pellet, made from powder calcined at 600 °C, ground by attrition (full line) or ground and fractionated (dotted line).

The density evolution, during sintering, of pellets made from powder after different calcination temperatures, was additionally studied by dilatometry. The relative density of pellets and the densification rate were computed from the experimental linear relative shrinkage[23] with an additional mass loss correction (TG data). The representative case of powder calcined at 600 °C is reported, as an example, in full line in Fig. 8a (relative density) and Fig. 8b (densification rate). It can be seen that the relative density curve presents a bend at ∼1320 °C.

The sintering of powder starts at 900 °C, which corresponds to the beginning of recrystallisation process in material. Above 900 °C the densification rate increases reaching a maximum at 1230 °C. However, at temperature higher than 1230 °C, the densification rate is decreasing abruptly (Fig. 8b). All pellets, independently of their calcination temperature, show similar behaviour during sintering.

The peculiarities of the morphological structure of pellets after sintering at different temperature were investigated by SEM, which revealed differences in densification of "hard" and "soft" agglomerates (Fig. 9). As shown in Fig. 9a, the annealing of pellets up to 1230 °C is accompanied by a full densification of "hard" agglomerates. They consist of close-packed particles with an average size of 0.3 μm. It seems

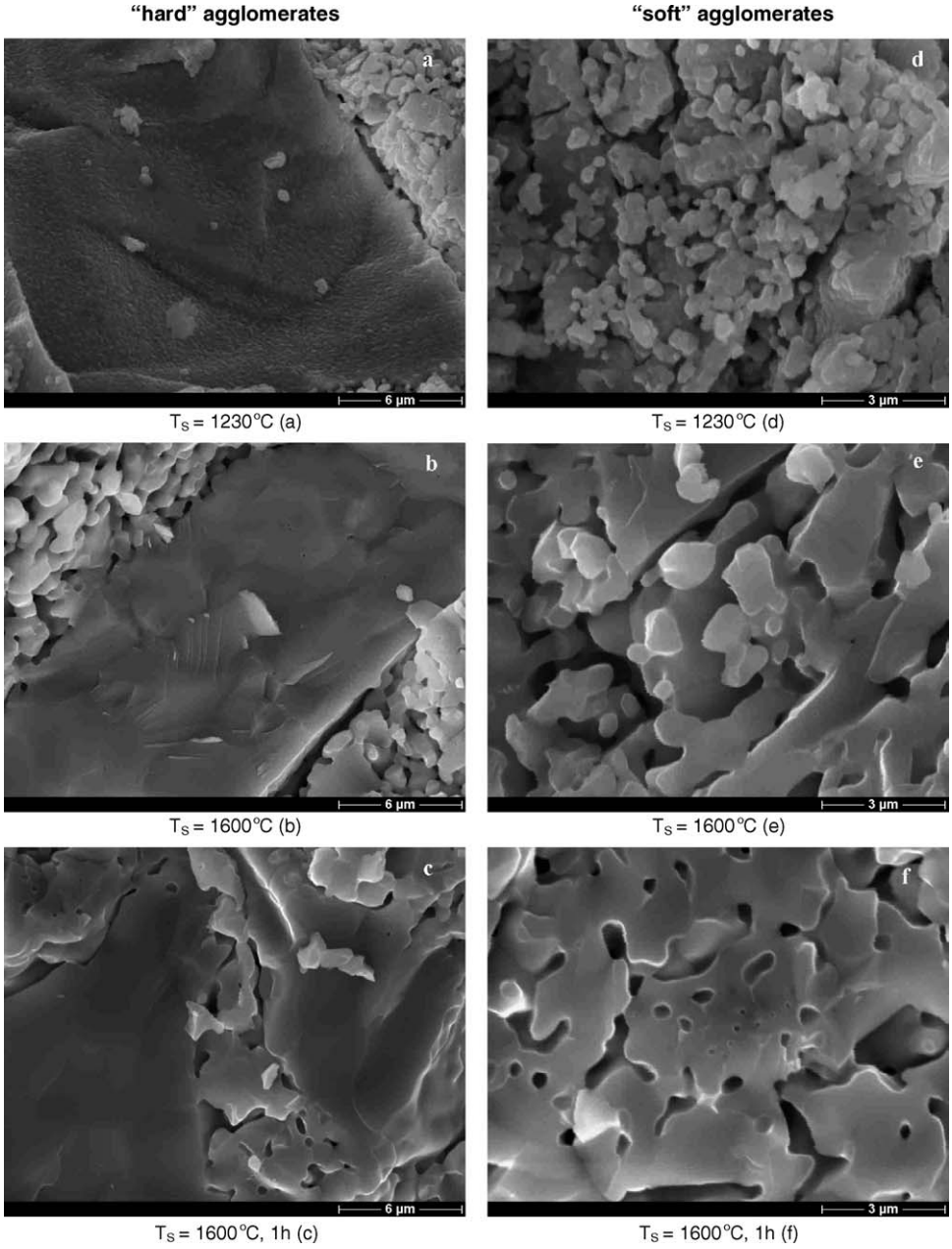

Fig. 9. SEM photographs of "hard" (a–c) and "soft" (d–f) components of Ce-YSZ pellet after shock sintering at 1230 °C, 1600 °C and after holding the temperature at 1600 °C for 1 h.

that the material sintering at low temperatures is determined by the high initial density of "hard" agglomerates, the small crystallite size ($L \sim 8$ nm at 600 °C) and the active surface of initial particles. On contrary, the annealing of soft agglomerates up to 1230 °C, also results in increase of particle size to 0.3 μm, but only in minor increase of the agglomerate density (Fig. 9d).

Subsequent heating up to 1600 °C is accompanied by a significant increase of crystallite size up to 2–4 μm for both types of agglomerates (Fig. 9b and e). Moreover, the soft agglomerates form typical necks. During heating, the different sintering behaviour between the soft and hard agglomerates is responsible for elongated pores formation along the hard agglomerates borders (Fig. 9b). These pores remains during the sintering stage along the grain boundaries (Fig. 10 a).

Annealing at 1600 °C for 1 h is accompanied by densification of material due to the sintering of "soft" agglomerates, which leads to a dense structure with closed submicron pores (Fig. 9c and f).

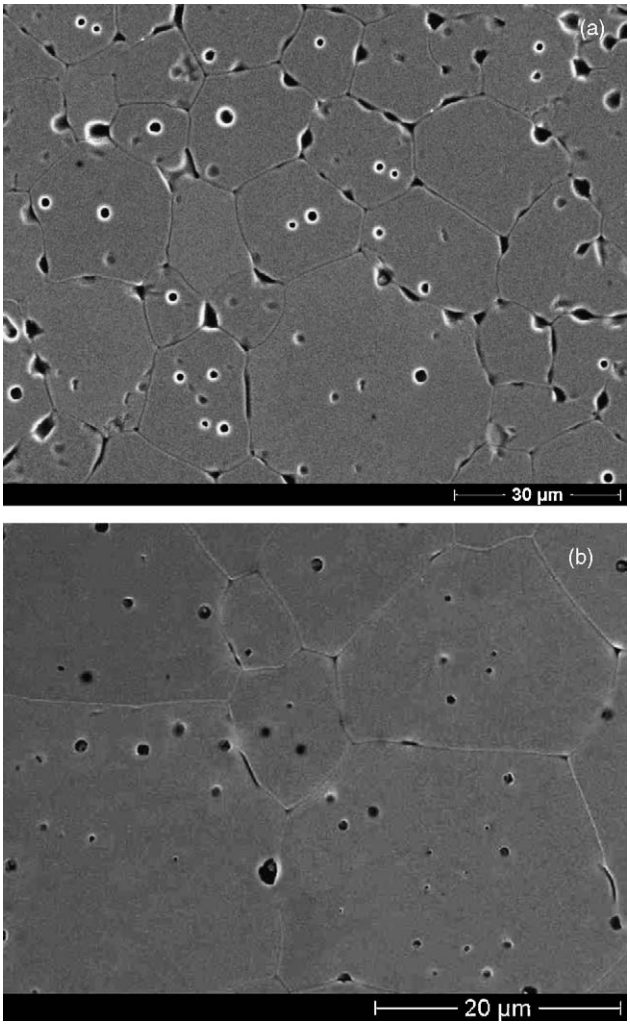

Fig. 10. SEM photograph of Ce-YSZ pellets made from ground (a) and from ground and fractionated powder (b).

According to these results and the literature,[24] the bend observed in the densification curve (Fig. 8a) for powder after grinding by attrition can be explained in the following way. At temperature up to 1230 °C the material densification takes place mainly by sintering of "hard" agglomerates and formation of a "rigid" skeletal structure in material. During following heating, the presence of this rigid framework hampers the sintering of "soft" agglomerates.

Therefore, to avoid the limitation of the sintering ability of powders by the "hard" agglomerates, pellets made from fine powders, containing a majority of "soft" and small agglomerates have been studied. Fine powders were produced by a fractionating method. The investigation of powder mass distribution by laser granulometry has shown that, after fractionating, 95 wt.% of agglomerates has an equivalent diameter less then 4 μm. Pellets produced from these powders had a density of 0.95–0.97 TD (Fig. 7).

It is important to note that after "mild" grinding by attrition, the weight fraction of fine powder strongly depends on the calcination temperature. So, after calcination at 110 °C, the fine powder fraction is 66% against 40% after calcination at 600 °C. However, when the powder is calcined at 1400 °C, the fine powder fraction drastically decreases to 2%. This is a consequence of the increase of agglomerates strength during the recrystallisation of material. Therefore, additional fractionating of fine agglomerates has a practical sense only for powders after low calcination temperature.

The density evolution of pellets made from fractionated powder after calcination at 600 °C (Fig. 8a) during sintering was also studied by dilatometry. The relative density and densification rates, as a function of the temperature, are reported in dotted lines in Fig. 8a and b, respectively. In this case, the sintering also starts at 900 °C and then the density continuously increases between 900 and 1450 °C. Only minor decrease of densification rates is observed above 1450 °C (Fig. 8b). Moreover, the final density of pellets made from fine fractionated powder is higher, although the initial density was lower then that of the agglomerated powder (Fig. 8a).

Apparently, during "mild" grinding by attrition of powder, the "soft" agglomerates mainly broke down. And, due to their lower effective density compared to the hard agglomerate, they concentrate in fine part powder fraction.

Moreover the absence of coarse "hard" agglomerates in the powder after fractionating leads to the absence of big pores in the sintered material (Fig. 10a). Therefore fine powders and "soft" agglomerates have similar sintering behaviour and the sintered material possesses a dense structure, well-formed grains and boundaries and homogeneously distributed submicron pores (Fig. 10b).

The densification behaviour of fine powder calcined at different temperatures (from 110 to 950 °C) was studied by dilatometry. The densification curves as a function of the temperature are displayed in Fig. 11. All curves can be divided in three temperature regions: from room temperature to 500 °C, from 500 to 900 °C and from 900 °C to 1600 °C.

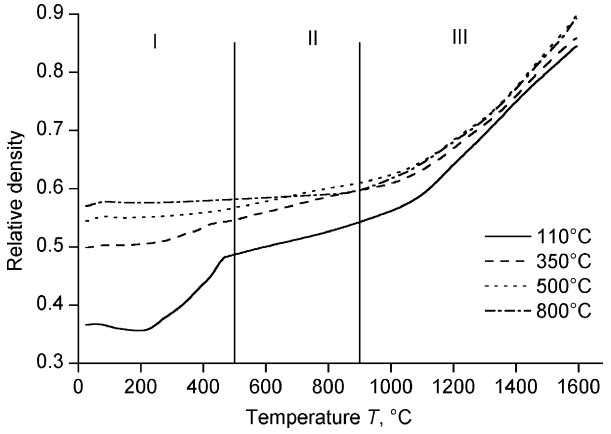

Fig. 11. Evolution with the annealing temperature of the relative density of Ce-YSZ pellet made from ground and fractionated powders calcined at 110, 350, 500 and 800 °C.

In the first region, from 200 to 500 °C, the density of pellets made from powders calcined at 110 °C or 350 °C, increases. This can be associated with the elimination of water from material which is responsible of a strong decrease of the pellets volume.

When the temperature increases from 500 to 900 °C, the pellets made from powders calcined at 110, 350 and 500 °C show a linear densification behaviour, which is associated with the material crystallisation and subsequent elimination of crystal water.

At the temperature of 900 °C and above, all powders densify similarly. The pellet densification is associated with recrystallization and sintering of material.

4. Conclusions

The thermal behaviour and the physical properties of the Ce-YSZ system as a function of the calcination temperatures were investigated in details.

After the synthesis by co-precipitation, the powder consists of "hard" and "soft" agglomerates with irregular shapes. Heating the powder between 370 and 660 °C transforms the system from an amorphous to a cubic face centred structure. This phase transition has a "stepwise" character and is accompanied by a double exothermic effect. The first exothermic effect is associated to the crystallisation of the matrix 16-YSZ with a ceria deficiency and the second peak is connected to the insertion (embedding) of the rest of ceria in the crystal lattice. During further heating, the recrystallisation processes (L) also take place and lead to agglomerate hardening. Calcination above 1265 °C is necessary to achieve a stable crystal structure.

The impact of the calcination temperature on the sintering ability of pellets was investigated in detailed. "Mild" methods like grinding by attrition, necessary for handling radioactive material, were used for pellet production. In this case, the powders after low-temperature treatment, from 110 °C up to 600 °C, present the best sinterability. Their small mean crystallite size (L) and high-level of lattice distortions ($\langle\varepsilon^2\rangle^{0.5}$) determine their high activity during sintering process. On contrary, after a calcination at temperatures higher than 600 °C, the recrystallisation process takes place and lead to agglomerates hardening. The powders consist of a majority of hard agglomerates and the dilatometry studies have demonstrated that the hard agglomerates control the sintering. They sinter at low temperatures (from 900 to 1230 °C) and then form a "rigid" skeletal structure which is hampered by the sintering of "soft" agglomerates at higher temperature. This sintering behaviour leads to the formation of cracks and pores along the grain boundaries.

So to avoid the limitation of sintering ability, pellets were performed from powder fractionated in acetone. The powder consists of a majority of soft agglomerates with an equivalent diameter of 4 μm. They form during sintering a dense microstructure with closed submicron pores. However, the fractionating method has a practical sense only after low calcination temperature because of the lower strength of agglomerates, which can be so broken more easily.

These different properties are interesting from a technological point of view. In fact, to obtain pellets with good properties, a low calcination temperature should be employed, simplifying the grinding step and increasing the rate of fractionating step.

Acknowledgement

This work has been supported by the European Union (EUROPART, contract no. F16W-CT-2003-508854).

The authors would like to express their thanks to W. Reichert for performing the XRD measurements and to M.M. Titov for SEM measurements.

References

1. Degueldre, C. and Paratte, J. M., Concept for an inert matrix fuel, an overview. *J. Nucl. Mater.*, 1999, **274**, 1–6.
2. Ledergerber, G., Degueldre, C., Heimgartner, P., Pouchon, M. A. and Kasemeyer, U., Inert matrix for the utilisation of plutonium. *Progr. Nucl. Energy*, 2001, **38**(3–4), 301–308.
3. Kuramoto, K., Mitamuro, T., Banba, T. and Muraoka, S., Development of ceramic waste forms for actinide-rich waste. *Progr. Nucl. Energy*, 1998, **32**(3–4), 509–516.
4. Gong, W. L., Lutze, W. and Ewing, R. C., Zirconia ceramics for excess weapons plutonium waste. *J. Nucl. Mater.*, 2000, **227**, 239–249.
5. Ronchi, C., Ottaviani, J. P., Degueldre, C. and Calabrese, R., Thermophysical properties of inert matrix fuels for actinide transmutation. *J. Nucl. Mater.*, 2003, **320**, 54–65.
6. Andrevskaya, E. R., Red'ko, V. P. and Lopato, L. M., Interaction of cerium oxide with hafnium, zirconium, and yttrium oxides at 1500 °C. *Powder Metallurgy Metal Ceram.*, 2001, **40**(7–8), 405–413.
7. Hinatsu, Y. and Muromura, T., Phase relations in the systems ZrO_2-Y_2O_3-Nd_2O_3 and ZrO_2-Y_2O_3-CeO_2. *Mat. Res. Bull.*, 1986, **21**, 1343–1349.

8. Maschio, S., Bacchiorrini, A. and Lucchini, E., Sintering behaviour of mechanically alloyed and coprecipitated 12Ce-PSZ powders. *J. Mater. Sci.*, 1998, **33**, 3437–3441.
9. Van de Graaf, M. A. C. G., Keizer, K. and Burggraaf, J. A., Influence of agglomerate structures in ultra-fine substituted zirconia powders on compaction and sintering behaviour. *Sci. Ceram.*, 1979, **10**, 83–92.
10. Kouzov, P. A., Basis for analysis of industrial dust and ground materials dispersion, Khimia, Leningrad, 1974, p. 280.
11. Barrier, D., Bukaemskiy, A. A., Soe, K. S., Titov, M. M. and Modolo, G., Fixation of actinides in zirconium based ceramics. In *Proceedings of the 9th International Conference on Environmental Remediation and Radioactive Waste Management, Nuclear Fuel Reprocessing and Waste Management*, 2003.
12. Williamson, G. K. and Hall, W. H., X-ray line broadening filed aluminium and wolfram. *Acta Metallurgica*, 1953, **1**, 22–31.
13. Klug, H. P. and Alexander, L. E., *X-Ray Diffraction Procedures for Polycrystalline and Amorphous Materials*. Wiley, New York, 1954, pp. 491–495.
14. Dodd, A. C. and McCornick, P. G., Synthesis and processing of ultrafine Mg-PSZ powder. *J. Metastable Nanocrystall. Mater.*, 1999, **312–314**, 221–226.
15. Aronne, A., Marotta, A., Pernice, P. and Catauro, M., Sol-gel processing and crystallisation of yttria-doped zirconia. *Thermochim. Acta*, 1996, **275**, 75–82.
16. Rossignol, S., Madier, Y. and Duprez, D., Preparation of zirconia-ceria materials by soft chemistry. *Catal. Today*, 1999, **50**, 261–270.
17. Ingo, G. M., Righini, G. and Scoppio, L., Chemical aspects in thermal treatment of ZrO_2-CeO_2-Y_2O_3 alloy. *Appl. Surf. Sci.*, 1992, **55–4**, 257–267.
18. Dzisko, V. A., *Basis of Catalysts Preparation Methods*, Nauka, Novosiborsk, 1983, p. 263.
19. Fernandez, A., Haas, D., Konings, R. J. M. and Somers, J., Fuel/target concepts for transmutation of actinides. In *Proceedings of the NEA P&T Exchange Meeting 2000*, Madrid, 2000.
20. Barrier, D., Bukaemskiy, A. A., Soe, K. S. and Modolo, G., Yttrium stabilized zirconium ceramic as host phase for actinides immobilization. In *Proceedings of the International Workshop on P&T and ADS development 2003*, SCK CEN Club House, Belgium, 2003.
21. Kinoshita, H., Kuramoto, K., Mazayoshi, U., Yanagi, T., Yamanaka, S., Mitamura, H. and Banba, T., Phase stability of yttria-stabilized zirconia with dissolved cerium and neptunium oxides under oxidizing and reducing atmospheres. *J. Am. Ceram. Soc.*, 2000, **83–2**, 391–396.
22. JCPDS, International Centre for Diffraction Date, 34-0394.
23. Kutty, T. R. G., Hedge, P. V., Khan, K. B., Basak, U., Pillai, S. N., Sengupta, A. K. *et al.*, Densification behaviour of UO2 in six different atmospheres. *J. Nucl. Mater.*, 2002, **305**, 159–168.
24. Dynys, F. W. and Halloran, J. W., Influence of aggregates on sintering. *J. Am. Ceram. Soc.*, 1984, **67–69**, 596–601.